Ka-band ARQ Using SNR Distributions Derived from Flight Data

David D. Morabito* and Kar-Ming Cheung*

ABSTRACT. — In previous studies, the technique of Automatic Repeat Request (ARQ) link analysis and planning was discussed in the context of effective data rate, throughput, latency, and frame error rate under the constraint that the signal-to-noise ratio (SNR) remains constant or has a Gaussian distribution during the ARQ communications session. Although these models may be valid at S-band (2.3 GHz) and X-band (8.4 GHz), they may not necessarily be valid for Ka-band (26 GHz or 32 GHz downlink) and optical links, where there is more variation due to atmosphere. Given that the constant SNR scenario may not be valid over a long time horizon and the Gaussian assumption may not be fully valid for flight conditions, we explored the ARQ channel using real SNR distributions derived from deep-space flight data acquired at Ka-band (32 GHz). In this report, we examine the Ka-band ARQ channel in the context of identifying optimum SNR settings and latency.

I. Introduction

The technique of Automatic Repeat Request (ARQ) link analysis and planning was previously discussed in the context of effective data rate, throughput, latency and frame error rate under the constraint that the signal-to-noise ratio (SNR) remains constant during the ARQ communications session [1–3]. ARQ systems make use of a feedback channel. These systems incorporate protocols that make requests for retransmission of data blocks whenever there are errors in reception. These systems trade time for link margin with the intent of returning all of the data. The constant SNR assumption may be plausible for S-band (2.3 GHz) and X-band (8.4 GHz) links, but may not necessarily be valid for Ka-band (e.g., 26 GHz and 32 GHz) and optical links, where one can incur large discrepancies in analysis and planning for these more dynamic SNR conditions. Given that the constant SNR approximation may not be valid over a long time horizon [4], a follow-up study was conducted to analyze the effect of varying SNR, such as that induced by the atmospheric channel [5]. This was because the assumption of a constant SNR during a tracking pass is not fully valid (such as for long-haul ARQ links) as the SNR likely changes during retransmissions of non-decodable frames (or frames that were not received). This study modeled signal level changes using a Gaussian distribution to model variations in received signal strength during a tracking pass [5].

* Communications Architectures and Research Section.

The research described in this publication was carried out by the Jet Propulsion Laboratory, California Institute of Technology, under a contract with the National Aeronautics and Space Administration.

Whereas the previous studies made use of constant SNR or Gaussian SNR assumptions, in this study we make use of actual SNR distributions (P_c/N_0 or E_b/N_0) derived from flight data of deep-space missions to model the ARQ channel.

The hypothetical ARQ link is considered "error-free" since all data frames will eventually be successfully received because there is no limit on the number of re-transmissions.[1] In this study, we consider a coded ARQ system using a low density parity check (LDPC) (1024, ½) code [6] operating under a dynamic link environment typical for Ka-band with different cases of SNR scatter. This link scenario is based on an analysis of a selective repeat "fast-varying" link. This technique assumes that SNRs in subsequent retransmissions of a code block can take on different values and are independent. Such is the case for the deep space link where the latency of the link is much longer than the coherence time of the atmospheric channel. The "slowly-varying" link (e.g., between the Earth and Moon) will be addressed in a future study.

In the previous study, the effect of changing SNR, or link uncertainty, was incorporated in the analysis of ARQ links where two limiting cases were examined [5]. These two cases consist of (a) a fast-varying SNR case when SNRs in subsequent re-transmissions of a code-block can assume different values and are independent, and (b) a slow-varying SNR case, when SNR values in subsequent re-transmissions of a code-block remain the same. Analytical expressions of effective SNR and latency for the two cases were derived. Then, the analysis was applied to the case of a coded ARQ system using the LDPC (1024, ½) code operating under dynamic link environments typical of a Ka-band link [5]. However, the analysis made use of Gaussian distributions and we know that actual distributions of SNR are not necessarily Gaussian.

Figure 1 displays the ARQ transmission and receiving timeline. Here T_{out} is the timespan from transmission to the time an acknowledgement is received at the transmitter as to the nature of the sent message. In order words, the latency. T_{out} consists of the sum of round-trip light time ($2T_c$) and any intervening latency due to processing delays at transmitter and receiver (Δ_T and Δ_R). P_{bk} is the frame error rate (FER) of the transmission channel and P_{ack} is the acknowledgement channel frame error rate (see [5]).

For this analysis, we wish to make use of distributions of actual SNR measurements from deep-space flight data. Hence, we retrieved several data sets of signal strength from previously analyzed Ka-band passes [7–8] and selected cases where the limiting causes of SNR variations were attributed primarily to atmosphere.

[1] A practical protocol will usually have a limit on the number of retransmissions.

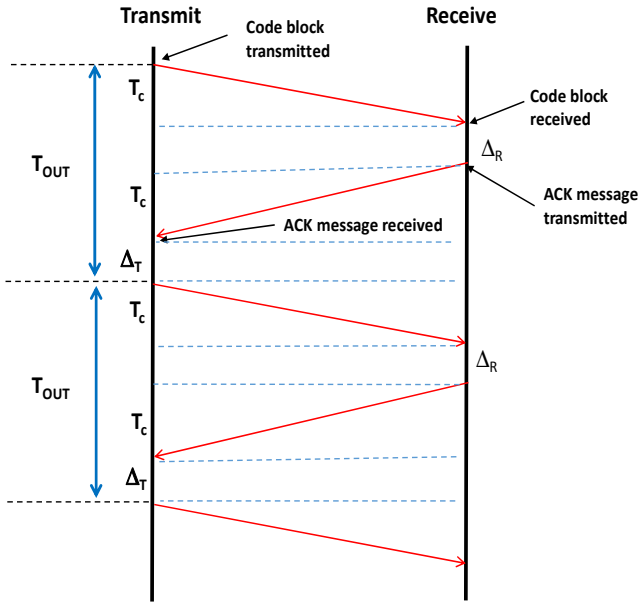

Figure 1. ARQ Transmission and Receiving Timeline

II. Model and Approach

The process that was followed involves generating the error-rate statistics of received SNR from actual data, denoted as $h(x|m)$ where $x = E_b/N_0$ (derived from P_c/N_0 measurements) and m represents different design point values for E_b/N_0. Here, P_c/N_0 is the carrier-to-noise spectral density ratio and E_b/N_0 is the bit energy-to-noise ratio. Cassini carrier-only signal strengths were converted to hypothetical E_b/N_0 using a link model involving nominal parameters such as data rate and telemetry modulation index of appropriate values. Kepler carrier P_c/N_0 measurements were converted to E_b/N_0 using the appropriate Kepler telemetry parameters (in lieu of using the direct Kepler E_b/N_0 measurements).

We next generate the frame error rate (FER) of the error correction code denoted by $f(x)$. For this study, we assumed an LDPC code rate of ½ and block size of 1024 [6], using equations provided in the Deep Space Network (DSN) Telecommunications Link Design Handbook [9].

We can calculate the mean error rate $\bar{e}(m)$ as [5]

$$\bar{e}(m) = \int_{-\infty}^{\infty} f(y)\,h(y|m)\,dy \tag{1}$$

which represents the effective error rate of a "send-once" link given $f(y)$ and $h(y|m)$.

The effective SNR is defined to be a hypothetical quantity whose increase over raw SNR represents the boost in energy per bit that one achieves by operating the link with ARQ. We calculate the effective SNR (E_b/N_0) for the case of a selective repeat ($N = 1$) and lossless acknowledgement channel link ($P_{ack} = 0$) (where N and P_{ack} are as defined in [5]):

$$\left(\frac{E_b}{N_0}\right)_{eff} = \left(\frac{E_b}{N_0}\right) + 10\log_{10}\left(1 + \frac{\bar{e}\left(\frac{E_b}{N_0}\right)}{1 - \bar{e}\left(\frac{E_b}{N_0}\right)}\right) \quad (2)$$

Here, the effective SNR, $(E_b/N_0)_{eff}$, and the design point SNR, E_b/N_0, are in units of dB. The process then involves calculating $(E_b/N_0)_{eff}$ for different values of E_b/N_0. We then locate the optimum operating design point SNR, (E_b/N_0), that corresponds to the minimum effective SNR, $(E_b/N_0)_{eff}$. The effective SNR is always a higher-valued quantity than the corresponding raw SNR. For passes with deep fades, the empirical density function, $h(y|m)$, will have non-Gaussian "expansive" asymmetric tails in the low-SNR region resulting in worse performance than that of a symmetric distribution.

The above expressions are valid for unlimited retransmission but would be different for truncated ARQ, which will not be addressed in this paper.

III. SNR Analysis

Figure 2 displays the cumulative distributions of Ka-band P_c/N_0 measurements from actual flight data [7–8] (solid curves) for individual passes, and those derived from a Gaussian model (dashed curves) using the mean and standard deviation derived from the flight data. Elevation angle dependence has not been removed from the data from which these distributions were derived. The family of distributions involving Kepler Ka-band carrier data lie to the right (with P_c/N_0 between 57 and 62 dB-Hz at 100% CD) and those for Cassini Ka-band lie to the left (with P_c/N_0 between 48 and 51 dB-Hz at 100% CD). Cassini was at a much longer range distance of ~8–10 AU (in orbit around at Saturn) while Kepler was much nearer ~1 AU (in Earth-trailing orbit) and thus the received power was higher for Kepler. Kepler had a telemetry link at 32 GHz Ka-band, while Cassini was carrier-only at Ka-band for radio science investigation purposes [10]. These data sets were not adjusted for space loss to a common range distance, but are left as is to allow for better visualization of the individual curves in Figure 2.

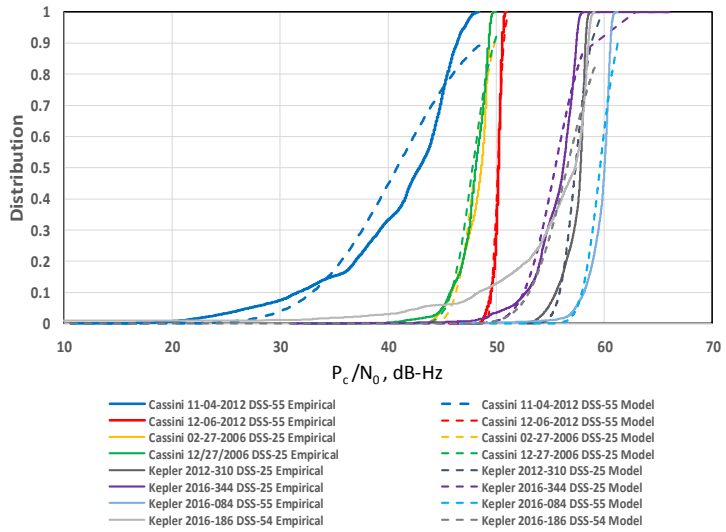

Figure 2. Cumulative distributions of P_c/N_0 for selected tracking passes; empirical (solid curves) and Gaussian model (dashed curves).

Figure 3 details the case of a non-empirical Gaussian distribution for SNR. Figure 3a shows the LDPC code's error rate $f(x)$ (purple), mean error rate $\bar{e}(x)$ (green) based on Equation (1), and the normalized probability density function (pdf) ($h(x|m)$) used in the Equation (1) integration where m is the SNR design point. In Figure 3a, we see the fully symmetric distribution where the Gaussian SNR has a standard deviation of 0.5 dB. This is in contrast to the distribution of most fair weather examples where tails are evident at the low SNR end of the distributions. Figure 3b displays the effective SNR versus raw SNR for this case, which is similar to the results presented in [5]. Here, the effective SNR value of 1.86 dB corresponds to the optimum (raw SNR) set-point of 1.63 dB. See the first three entries in Table 1, which provides the results for Gaussian distributions with standard deviations of 0.5, 1.0 dB, and 1.5 dB.

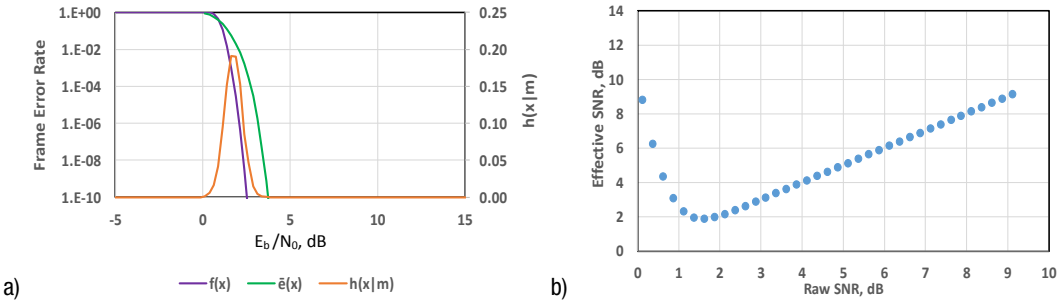

Figure 3. Gaussian model with 0.5 dB standard deviation a) $f(x)$, $\bar{e}(x)$ and pdf ($h(x|m)$ = Gaussian), b) effective SNR versus raw SNR.

For our non-Gaussian SNR analysis in this article, we take the set of measured P_c/N_0 signal strengths over a tracking pass. We remove a nominal data channel model to obtain a set of estimated E_b/N_0 values from which we derive a pdf. We then examine the individual pass results using the formulation in Section II.

We first consider a case involving a fair-weather Kepler pass conducted on 2016-084[2] with DSS-55.[3] Figure 4a shows the LDPC code's error rate $f(x)$ (purple), mean error rate $\bar{e}(x)$ (green) based on Equation (1), and the normalized pdf ($h(x|m)$) used in the Equation (1) integration where x is the SNR design point. For the purpose of this exercise, we choose the design point to be the E_b/N_0 corresponding to the peak of the density function. For Figure 4a, we show the pdf corresponding to its peak, which occurs at the optimum design point of E_b/N_0 ~2.1 dB. Here we see a "small" tail lying to the left of the otherwise symmetric pdf, which distinguishes it from the perfectly symmetric pdf of a Gaussian SNR distribution (see Figure 3a). The integration using Equations (1–2) is repeated for a wide range of design points. Figure 4b displays the effective SNR versus raw SNR for all of these design points for pass 2016-084 involving DSN station DSS-55. Here, the minimum effective SNR is about 3.1 dB occurring at a raw SNR near 2.1 dB, consistent with results

[2] Here the designation for a tracking pass date is shown as "Year-DOY" where DOY denotes the day-of-year of the tracking pass.

[3] Here the designation for a deep-space tracking station is shown as DSS-id, where id is the station designation. Goldstone designations can be denoted as 25 or 26, Canberra designations as 34, 35, or 36, and Madrid designations as 54 or 55. These passes involve the use of beam-waveguide antennas that accommodate downlink Ka-band operations.

shown in Table 2 of Cheung and Choi 2016 [5], and this represents the optimum design point.

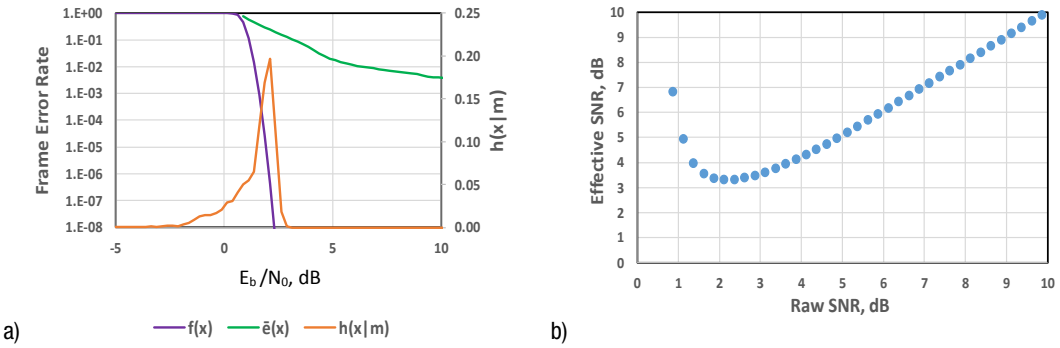

Figure 4. Kepler pass 2016-084 with DSS-55 a) $f(x)$, $\bar{e}(x)$ and pdf ($h(x|m)$), b) effective SNR versus raw SNR.

Next, we consider the case of a tracking pass involving more variable or turbulent weather conditions; a rainy weather pass conducted with Cassini on November 4, 2012, which involved tracking station DSS-55 in Madrid, Spain. Figure 5a displays the LDPC code's error rate $f(x)$ (purple), mean error rate $\bar{e}(x)$ (green) using Equation (1), and the normalized pdf $h(x|m)$ used in the Equation (1) integration of the Cassini signal strength data where x is the E_b/N_0 SNR design point (chosen to be $x = 7$ dB for the case of this plot). We choose the design point to be the E_b/N_0 corresponding to the peak of the density function. For this case, we see extended tails in both directions away from the peak of the SNR pdf, characteristic of passes with significant SNR variation, such as due to turbulent or rainy weather events. Figure 5b displays the effective SNR versus the raw SNR for all design points considered. Here the minimum effective SNR is about 5.3 dB occurring at a raw SNR near 1 to 2 dB. We see here that the SNR pdf exhibits a much wider range of values, including the feature of asymmetric tails. Note that the effective SNR versus raw SNR curve in Figure 5b shows a flattening where the minimum occurs. In this case, the identification of a definitive minimum is difficult to immediately discern.

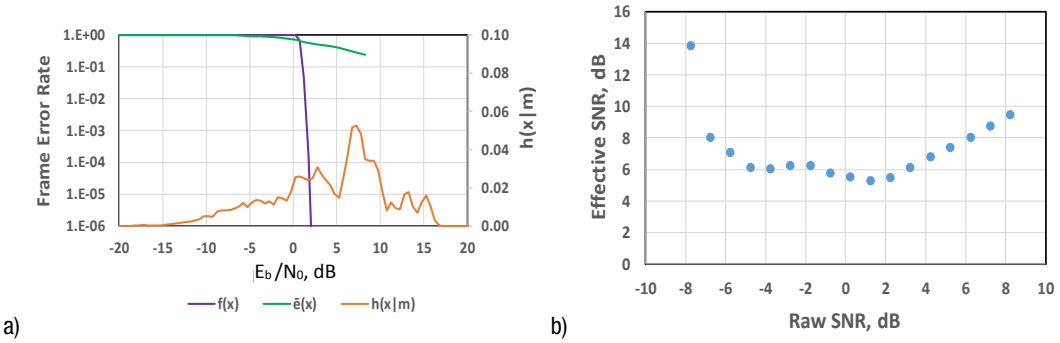

Figure 5. Cassini pass 11-04-2012 with DSS-55 a) $f(x)$, $\bar{e}(x)$ and pdf ($h(x|m)$), b) effective SNR versus raw SNR.

Additional cases involving empirical distributions from DSN tracking passes are displayed in Figures 6–11. Figures 6–7 show other examples of cases where the signal strength pdf is a

fairly narrow characteristic of fair weather passes such as shown in Figure 4. Here there is usually a sharp drop on signal strength in the high end but some tail in the lower end of the distribution either due to changes in weather, elevation angle, or non-atmospheric effects such as variations in pointing. The presence of this tail, even in cases of good weather, distinguishes the SNR flight data distribution from that of a perfectly symmetric non-empirical distribution such as that of a Gaussian model (see Figure 3a). For the case of empirical data, there may be effects due to a changing elevation angle that have not been normalized (or adjusted out) for this study. For Kepler tracking pass 2016-344 at DSS-36, we see the minimum effective SNR is 2.65 dB occurring at a raw SNR of 1.875 dB (see Figure 6b). For Kepler pass 2012-311 conducted at DSS-34, the minimum effective SNR is 3.271 dB occurs at a Raw SNR of 2.375 dB (see Figure 7b).

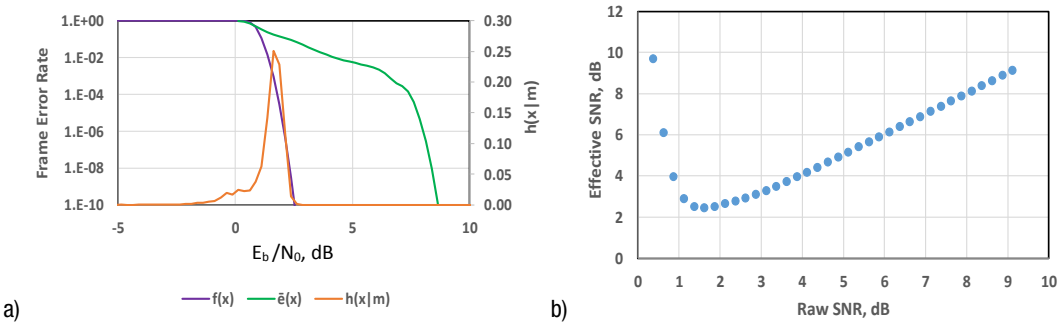

Figure 6. Kepler pass 2016-344 conducted at DSS-36 a) $f(x)$, $\bar{e}(x)$ and pdf ($h(x|m)$), b) effective SNR vs. raw SNR.

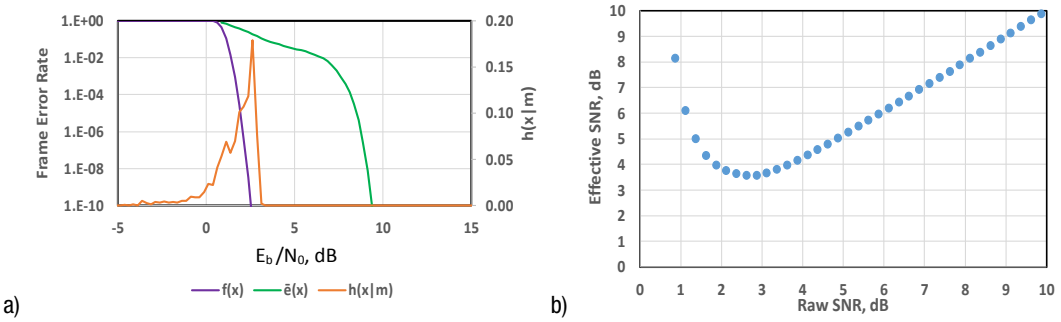

Figure 7. Kepler pass 2012-311 conducted at DSS-34 a) $f(x)$, $\bar{e}(x)$ and pdf ($h(x|m)$), b) effective SNR vs. raw SNR.

Figures 8–11 show examples of cases where the signal strength pdf is wider, which is characteristic of turbulent or rainy weather passes, such as depicted in Figure 5. Here, there could be tails at either end of the pdf (such as in Figure 5a) but with wider tails at the lower end of the distributions due to significant variation caused by weather. The minimum effective SNRs run on the order of 5 dB or higher. Sometimes, there are non-atmospheric effects such as pointing coming into play. In addition, the effective SNR versus raw SNR curves exhibit some flattening around the minimum SNR, where it is sometimes difficult to decipher the location of the true minimum.

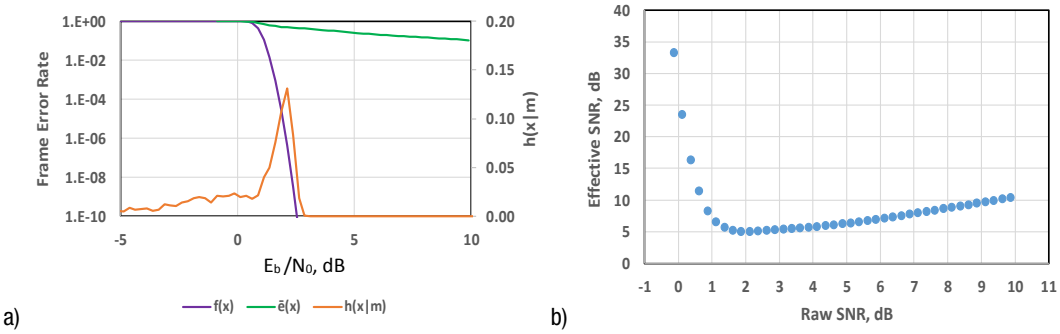

Figure 8. Kepler pass 2016-186 conducted at DSS-54 a) $f(x)$, $\bar{e}(x)$ and pdf ($h(x|m)$), b) effective SNR vs. raw SNR.

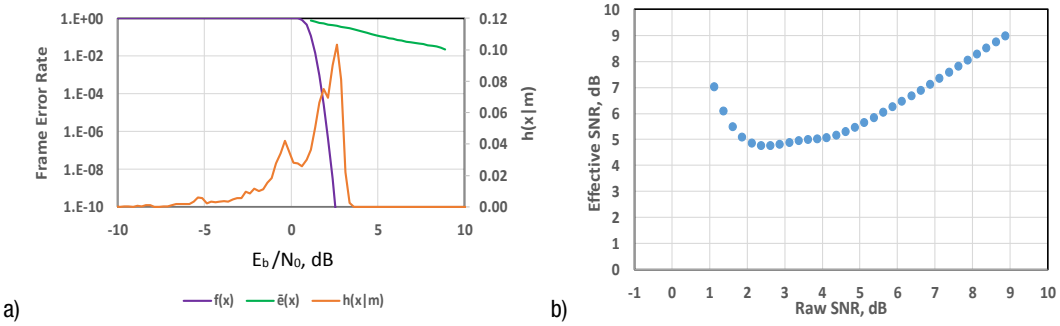

Figure 9. Kepler pass 2016-344 conducted at DSS-25 a) $f(x)$, $\bar{e}(x)$ and pdf ($h(x|m)$), b) effective SNR vs. raw SNR.

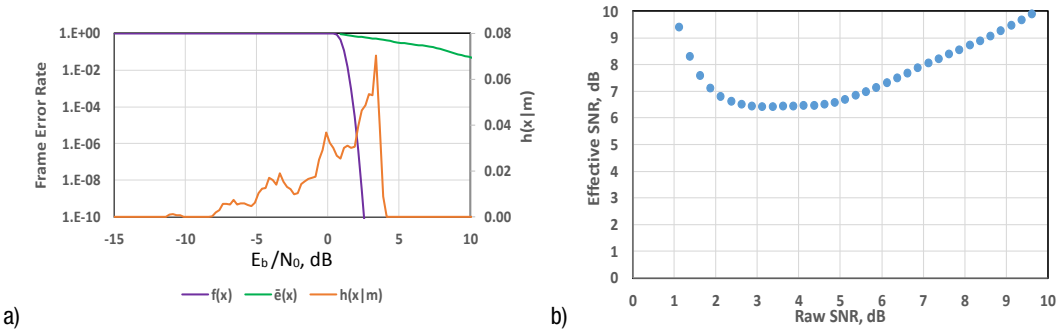

Figure 10. Kepler pass 2016-265 conducted at DSS-35 a) $f(x)$, $\bar{e}(x)$ and pdf ($h(x|m)$), b) effective SNR vs. raw SNR.

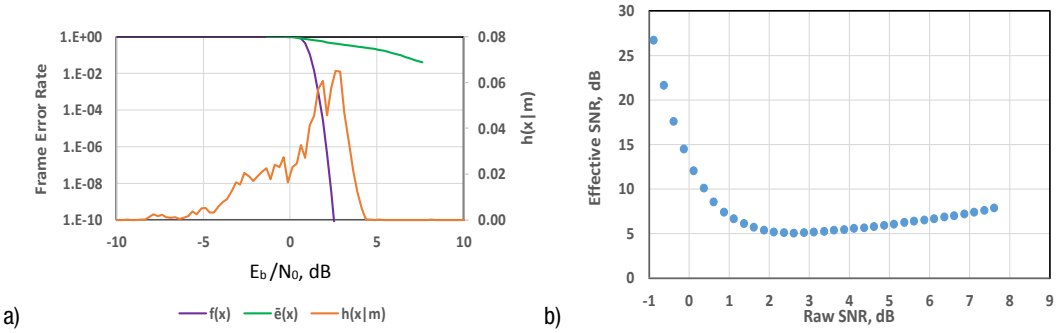

Figure 11. Kepler pass 2017-064 conducted at DSS-36 a) $f(x)$, $\bar{e}(x)$ and pdf ($h(x|m)$), b) effective SNR vs. raw SNR.

Table 1 summarizes the results for several tracking passes as well as three non-empirical cases of Gaussian distributions with standard deviations of 0.5, 1.0, and 1.5 dB. The first column denotes a Case ID, where the Gaussian cases are denoted as "Gauss x.x", where x.x denotes the standard deviation in dB for the Gaussian SNR distribution. For the cases involving passes where SNRs were derived from real flight data, the Case ID is represented as "Year-DOY", where Year denotes the year of the tracking pass, and DOY denotes the day-of-year that the pass was conducted. The DSS column denotes the deep-space tracking station used to acquire the signal data (blank for Gaussian cases). Also shown are the effective SNR and raw SNR at the optimum design point, the standard deviation of the P_c/N_0 data set measurements, and the corresponding frame error rate (see [5]).

Table 1. Individual Pass Results and Gaussian Cases

Case ID	DSS	Effective SNR, dB	Raw SNR, dB	Std. Dev. db-Hz	FER at min SNR
Gauss 0.5		1.86	1.63	0.50	0.05
Gauss 1.0		2.76	2.13	1.00	0.14
Gauss 1.5		3.38	2.38	1.50	0.21
2016-344	36	2.43	1.63	0.69	0.17
2017-064	36	5.03	2.63	2.06	0.43
2016-264	35	3.65	2.13	1.23	0.30
2016-265	35	6.41	3.38	2.52	0.50
2012-311	34	3.56	2.63	0.99	0.19
2016-345	34	3.45	1.88	1.15	0.30
2016-084	55	3.31	2.13	0.94	0.24
2016-186	54	5.01	2.13	2.50	0.48
2012-310	25	3.37	1.88	0.96	0.29
2016-344	25	4.75	2.38	1.65	0.42
2016-083	25	1.82	1.63	0.32	0.04
2016-140	25	2.36	1.88	0.71	0.10
2011-034	25	1.46	1.38	0.33	0.02
2011-075	25	3.29	2.38	0.85	0.19
2011-240	25	2.38	1.88	0.65	0.11
2012-004	25	3.09	2.38	0.74	0.15
2012-032	25	2.66	2.13	0.92	0.12
2013-342	25	2.18	1.88	0.46	0.07
2013-011	25	1.90	1.38	0.38	0.11
2013-028	25	2.81	2.13	0.74	0.15
2013-066	25	2.03	1.63	0.42	0.09
2013-147	25	1.83	1.38	0.73	0.10

Upon examination of Table 1, the effective SNRs for the flight data distribution cases typically run higher than those of the equivalent Gaussian cases. For example, we see that pass 2016-084 (with DSS-55) has a comparable standard deviation of 0.94 dB with that of the Gaussian case with a standard deviation of 1.0 dB. However, pass 2016-084 has a somewhat higher effective SNR of 3.31 dB versus the 2.76 dB effective SNR of the Gaussian

case. Another example shows that pass 2013-342 (with DSS-25) has a comparable standard deviation of 0.46 dB with that of the Gaussian case with a standard deviation of 0.5 dB. However, pass 2013-342 has a somewhat higher effective SNR of 2.18 dB versus the 1.86 dB effective SNR of the Gaussian case.

Figure 12 depicts the multi-pass effective SNR versus raw SNR for each pass at the minimum effective SNR, as well as that of the Gaussian non-empirical cases. Here we see a roughly linear dependence at the low values which exhibits more scatter at higher SNR values. Note that the three Gaussian distribution cases (purple) line up well with the clearer-weather tracking station passes at low SNR (mostly Goldstone passes). Only when the pass is operated in near perfect weather conditions does the density function approach that of a Gaussian (but with some tail). Figure 13 depicts the standard deviation estimated from the P_c/N_0 measurements over each tracking pass versus the effective SNR. Note that there is a roughly linear trend of standard deviation versus effective SNR. Figure 14 depicts frame error rate versus minimum effective SNR. The frame error rate of about 0.05 at the lowest effective SNRs is consistent with the results from a previous study [5]. However, we also see very high frame error rates reaching as high as 0.5. Such frame error rates seem excessive for nominal operations, but could be tolerable using the ARQ protocol, where one would pay a price in increased latency (see Section IV).

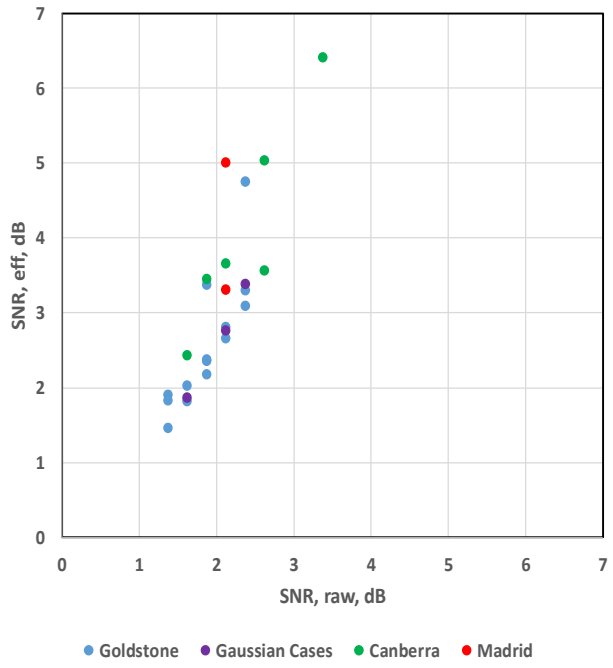

Figure 12. Effective SNR versus raw SNR for each pass as well as the three Gaussian distribution cases (see legend).

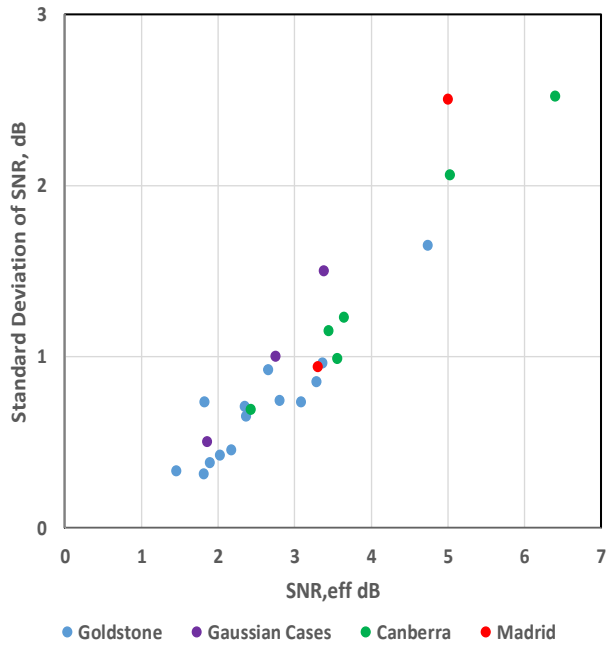

Figure 13. Standard deviation of P_c/N_0 versus effective SNR.

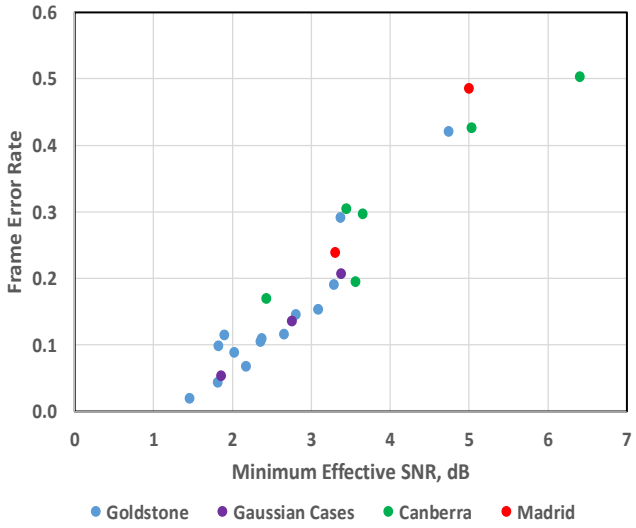

Figure 14. Frame error rate versus minimum effective SNR.

IV. Latency Analysis

One penalty for the ARQ link includes increased latency for retransmission. Here we will be discussing the statistical Latency for our "fast-varying" ARQ System. The mean latency, L_{fast}, as a function of E_b/N_0 is given by [5]

$$L_{fast}\left(E_b / N_0\right) = T_c + \left[\left(1-\theta\right)/\theta\right] T_{out} \tag{3}$$

where T_c is the one-way light time, $\theta = [1 - \bar{e}\,(E_b/N_0)](1 - P_{ack})$, T_{out} is the single transmission latency acknowledgement depicted in Figure 1 and P_{ack} is probability of acknowledgement. Here, E_b/N_0 was assumed to have a Gaussian distribution with standard deviation σ [5]. In this article, we use E_b/N_0 distributions based on actual flight data. We consider a coded ARQ system using LDPC (1024, 1/2) operating under a dynamic link environment that is typical for Ka-band with different cases of σ. We will again assume a lossless acknowledgement link ($P_{ack} = 0$). We also assume that processing latency is small compared to light-time delay. Thus, normalizing Equation (3) by T_{out} results in a floor of 0.5 for high SNR.

Several latency versus raw SNR curves using Equation (3) are shown in Figure 15 (where latency is normalized by T_{out}). These include curves for pass 2013-147 involving DSS-25 (dashed blue), pass 2016-344 involving DSS-25 (dashed yellow), pass 2011-034 involving DSS-25 (dashed light green), pass 2016-345 involving DSS-34 (dashed purple), and two for the theoretical cases of a Gaussian distributions with SNR standard deviations of 0.5 dB-Hz (dashed black) and 1.5 dB-Hz (solid black). The Gaussian curve with a standard deviation of 1.5 dB-Hz lies mostly in between the curves of non-Gaussian cases based on actual flight signal data, where lower scatters lie to the left and higher scatters lie to the right of it at higher SNRs.

The 2016-344 pass showed a very highly spread-out asymmetric SNR distribution characteristic of turbulent weather conditions (Figure 9a), whereas those for 2013-147 and 2011-034 were more representative of typical clear weather conditions. For a given SNR and T_{out}, we see that the turbulent weather cases (2016-345 DSS-34 and 2016-344 DSS-25) will have a significantly higher latency at small SNRs. As SNR increases to higher values, latency becomes small and less significant for all cases, reaching the floor of 0.5. Thus, when there is sufficient SNR allowing the data to be successfully received and acknowledged, the latency of 0.5 corresponds to a one-way light time. As the SNR becomes very small, one may need to wait several round-trip light times before achieving successful reception and acknowledgement.

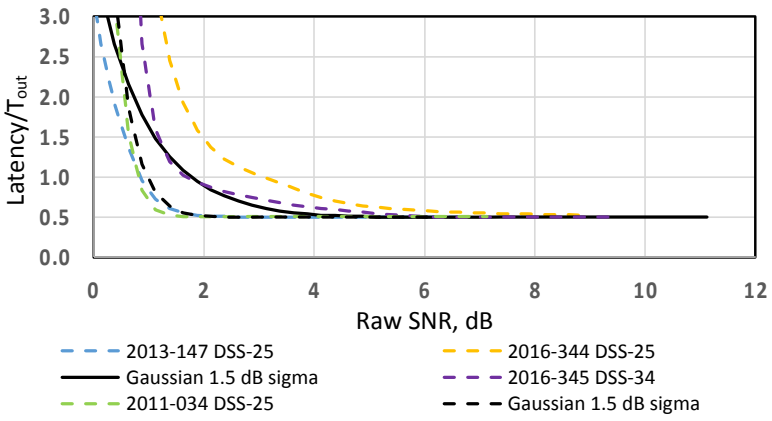

Figure 15. Normalized latency versus raw SNR for several passes (dashed colors) and for two Gaussian cases (black curves). See legend.

V. Conclusion

In previous studies, the technique of ARQ link analysis and planning was discussed in the context of effective data rate, throughput, latency and frame error rate under the constraint that the SNR remains constant or has a Gaussian distribution during the ARQ communications session. Given that the constant SNR scenario may not be valid over a long time horizon and the Gaussian assumption may not be fully valid, we explored the ARQ channel using real SNR distributions derived from deep-space flight data. We found that for nominally clear weather conditions, the SNR distribution more closely approximated a Gaussian distribution, but usually included tails at the lower SNR end. Under conditions of turbulent or heavy weather conditions, there was more spread in the distributions, including larger tails and in some cases tails at the high SNR end of the distributions. We examined the effective SNR versus raw SNR curves to identify where the minimum effective SNR occurred that defined the optimum set point in raw SNR. It was found that for clear weather passes, there were easily defined minimums. For more turbulent weather passes there was some flattening in the region of the minimum making it sometimes difficult to discern a clear minimum. The choice of an optimum set point for turbulent weather conditions may thus involve a wide range of SNRs in which to operate which therefore involves tradeoffs to consider.

Latency for the ARQ link was also examined and it was found that for lower SNRs, the turbulent weather passes would experience higher latencies than clear weather passes. At high SNRs, latencies were lower and similar over all weather conditions.

Acknowledgements

We appreciate the support provided by Faramaz Davarian of JPL for conducting this study; Marcie Smith at NASA Ames Research Center for assistance in providing the Kepler Ka-band data sets used in this as well as earlier studies; and the Cassini Radio Science Team for their support in providing the data sets for this as well as for earlier studies. We also would like to thank Sam Dolinar of JPL for providing a thorough review of this paper.

References

[1] F. Pollara and L. Ekroot, "Analysis of Automatic Repeat Request Methods for Deep-Space Downlinks," *The Telecommunications and Data Acquisition Progress Report,* vol. 42-122, Jet Propulsion Laboratory, Pasadena, California, pp. 66–83, August 15, 1995. https://ipnpr.jpl.nasa.gov/progress_report/42-122/122L.pdf

[2] K. Cheung, "Problem Formulation and Analysis of the 1-Hop ARQ Links," *The Interplanetary Network Progress Report,* vol. 42-194, Jet Propulsion Laboratory, Pasadena, California, pp. 1–15, August 15, 2013. https://ipnpr.jpl.nasa.gov/progress_report/42-194/194A.pdf

[3] K. Cheung, C. Lau, C. Lee, "Link Analysis for Space Communication Links Using ARQ Protocol," IEEE Aerospace Conference 2014, Big Sky, Montana, March 2014.

[4] K. Cheung, "The Role of Margin in Link Planning and Optimization," IEEE Aerospace Conference 2015, Big Sky, Montana, March 2015.

[5] K. Cheung and T. Choi, "Statistical ARQ Link Analysis and Planning for Dynamic Links," IEEE Aerospace Conference 2016, Big Sky, MT, 2016, pp. 1–8. doi: 10.1109/AERO.2016.7500547. https://ieeexplore.ieee.org/document/7500547

[6] K. S. Andrews, D. Divsalar, S. Dolinar, J. Hamkins, C. R. Jones, and F. Pollara, "The Development of Turbo and LDPC Codes for Deep-Space Applications," in *Proceedings of the IEEE,* vol. 95, no. 11, pp. 2142–2156, November 2007. doi: 10.1109/JPROC.2007.905132. https://ieeexplore.ieee.org/document/4383367

[7] D. D. Morabito, "Deep-Space Ka-Band Flight Experience," *The Interplanetary Network Progress Report,* vol. 42-211, Jet Propulsion Laboratory, Pasadena, California, pp. 1–16, November 15, 2017. https://ipnpr.jpl.nasa.gov/progress_report/42-211/211B.pdf

[8] D. D. Morabito, D. Kahan, K. Oudrhiri, and C.-A. Lee, "Cassini Downlink Ka-Band Carrier Signal Analysis," *The Interplanetary Progress Report,* vol. 42-208, Jet Propulsion Laboratory, Pasadena, California, pp. 1–22, February 15, 2017. http://ipnpr.jpl.nasa.gov/progress_report/42-208/208B.pdf

[9] DSN Telecommunications Link Design Handbook, "34-m and 70-m Telemetry Reception," DSN No. 810-005, Station Data Processing, Module 207, Rev. A, Jet Propulsion Laboratory, Pasadena, California, June 13, 2003. https://deepspace2.jpl.nasa.gov/dsndocs/810-005/207/207A.pdf

[10] A. Kliore, J. Anderson, J. Armstrong, S. Asmar, C. Hamilton, et al., "Cassini Radio Science," *Space Science Reviews,* vol. 115, no. 1–4, pp. 1–70, November 2004. https://link.springer.com/article/10.1007/s11214-004-1436-y#enumeration